ChemComm

COMMUNICATION

View Article Online
View Journal | View Issue

Cite this: *Chem. Commun.*, 2019, 55, 628

Received 24th October 2018,
Accepted 7th December 2018

DOI: 10.1039/c8cc08517j

rsc.li/chemcomm

Metal support effects in electrocatalysis at hexagonal boron nitride†

Dan-Qing Liu, ‡[a] Binglin Tao,‡[a] Hong-Cheng Ruan,‡[b] Cameron L. Bentley *[a] and Patrick R. Unwin *[a]

A scanning electrochemical droplet cell technique has been employed to screen the intrinsic electrocatalytic hydrogen evolution reaction (HER) activity of hexagonal boron nitride (h-BN) nanosheets supported on different metal substrates (Cu and Au). Local (spatially-resolved) voltammetry and Tafel analysis reveal that electronic interaction with the underlying metal substrate plays a significant role in modulating the electrocatalytic activity of h-BN, with Au-supported h-BN exhibiting significantly enhanced HER charge-transfer kinetics (exchange current is *ca.* two orders of magnitude larger) compared to Cu-supported h-BN, making the former material the superior support in a catalytic sense.

Electrochemical water splitting is widely recognized as the most sustainable method for generating hydrogen (H_2), a fuel that is in growing demand[1] for use in green energy technologies (*e.g.*, fuel cells) as the world moves towards a decarbonized future.[2] Noble metal based materials (*e.g.*, Pt) are the most efficient HER electrocatalysts in aqueous acid media, with fast electrode reaction kinetics resulting in low overpotentials.[3] However, due to the high cost and relative scarcity of these materials, there is an ongoing search for cheap, earth-abundant HER electrocatalysts, for example, two-dimensional (2D) materials such as transition metal dichalcogenides,[4] carbon nitride,[5] and sandwich structures based on 2D crystals,[6] which in recent years have shown great promise, with certain classes exhibiting considerable catalytic activity and high (electro)chemical stability.[7] Although it is intrinsically insulating (*i.e.*, band gap of 3.6 to 7.1 eV),[8] hexagonal boron nitride (h-BN) has attracted considerable attention in oxygen reduction reaction (ORR)[9,10] and hydrogen evolution reaction (HER) catalysis.[11] This is because the band gap of monolayer h-BN can be considerably reduced by introducing defects such as B/N vacancies and impurities,[12] and tuned to an extent through decoration with hydrogen atoms.[13] Moreover, as electron tunneling through ultrathin h-BN layers is possible,[14] electronic interaction with the underlying metal support substrate (*i.e.*, through mixing of the d_{z^2} metal orbitals with the N-p_z and B-p_z orbitals of h-BN) can tune electrochemical (electrocatalytic) activity.[15]

In this study, we explore the tunable electronic properties of h-BN in the context of (electro)catalysis by considering the HER activity of as-grown h-BN nanosheets supported on Cu (denoted as h-BN/Cu) and Au (denoted as h-BN/Au) substrates. The intrinsic electrocatalytic properties of h-BN have been probed using scanning electrochemical cell microscopy (SECCM, see Fig. 1a),[16,17] a scanning droplet cell technique that allows characteristic surface sites (*e.g.*, h-BN *vs.* metal substrate surface, herein) to be targeted and electrochemically characterized at the 'single-entity' level.[16–18] SECCM has been deployed in the voltammetric hopping mode,[18–20] where the droplet (meniscus) cell formed at the end of an electrolyte-filled (0.1 M $HClO_4$, herein) nanopipet (tip diameter, d_t = 150 to 300 nm, herein) is approached to (contacted with) the sample (working electrode) surface sequentially at a series of predefined locations, and upon each landing a spatially-resolved linear-sweep voltammogram (LSV) is recorded (further detail available in the ESI,† Section S1). In other words, in a single SECCM experiment, hundreds of spatially-independent nano-electrochemical cells are formed, with the probed area defined by the footprint of the meniscus (droplet) cell, allowing the HER activity of individual h-BN nanosheets to be compared and visualized directly, providing new insights into the catalytic properties of these promising non-precious metal electrocatalysts.

As detailed in Section S1 of the ESI,† the h-BN nanosheets were grown on polycrystalline Cu foils (h-BN/Cu) by an atmospheric pressure chemical vapour deposition (CVD) method.[21] The as-grown h-BN was subsequently transferred onto the Au substrate (h-BN/Au) by a polymethyl-methacrylate (PMMA) method.[22] The morphologies of as-grown h-BN/Cu and transferred h-BN/Au were observed directly by field emission scanning electron

[a] *Department of Chemistry, University of Warwick, Gibbet Hill Road, Coventry, UK. E-mail: c.bentley.1@warwick.ac.uk, p.r.unwin@warwick.ac.uk*
[b] *School of Information and Safety Engineering, Zhongnan University of Economics and Law, Wuhan 430073, China*

† Electronic supplementary information (ESI) available: Materials and methods (S1), LSVs obtained in the presence and absence of air (S2) and LSVs obtained on the metal (Cu and Au) support surfaces (S3). See DOI: 10.1039/c8cc08517j

‡ These authors contributed equally to this work.

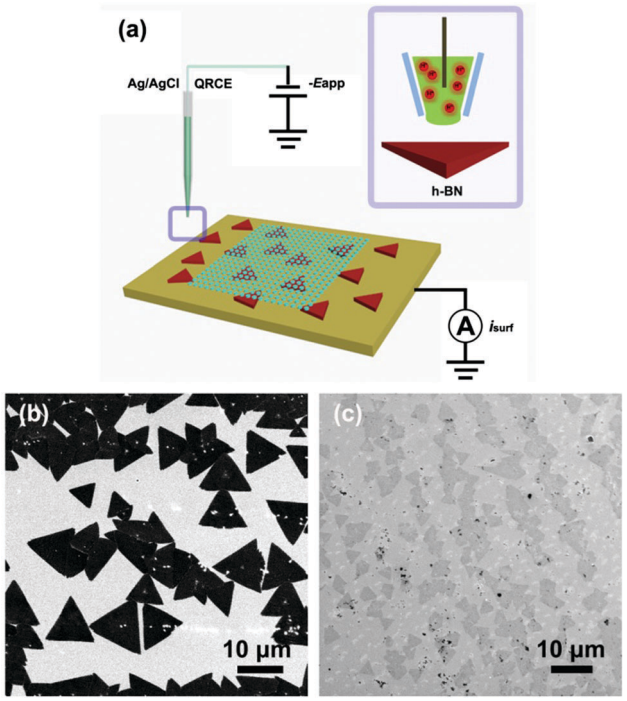

Fig. 1 (a) Schematic showing the scanning electrochemical cell microscopy (SECCM) set up used to screen the catalytic activity of h-BN at the nanoscale. Potential, $-E_{app}$, is applied to the Ag/AgCl quasi-reference counter electrode (QRCE) in the nanopipet probe and current, i_{surf}, is measured at the substrate (working electrode). Inset is an enlarged diagram of the probed h-BN interface during a single 'hop' of a scanning experiment. FE-SEM images of (b) as-grown h-BN/Cu and (c) transferred h-BN/Au.

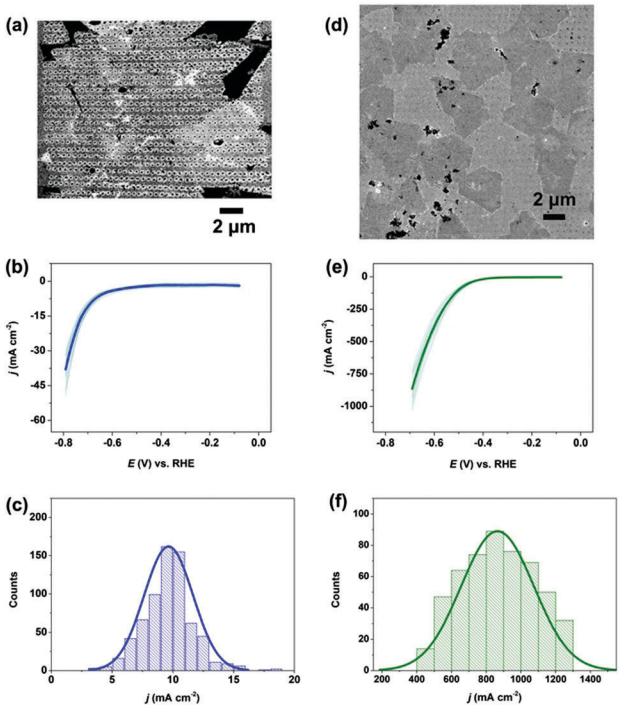

Fig. 2 (a) FE-SEM image of an area of the h-BN/Cu scanned using SECCM (individual droplet footprints are visible). (b) Representative LSVs (transparent) obtained from 45 points across the surface of h-BN/Cu and average LSV (blue) obtained from all points on h-BN/Cu (684 individual measurements). (c) Histogram (N = 684) showing the distribution in j values measured at the surface of h-BN/Cu at an applied potential of −0.688 V *vs.* RHE. (d) FE-SEM image of an area of the h-BN/Au scanned using SECCM (individual droplet footprints are visible). (e) Representative LSVs (transparent) obtained from 35 points across the surface of h-BN/Au and average LSV (green) obtained from all points on h-BN/Au (515 individual measurements). (f) Histogram (N = 515) showing the distribution in j values measured at the surface of h-BN/Au at an applied potential of −0.688 V *vs.* RHE. All LSVs were obtained from a 0.1 M $HClO_4$ solution at a voltammetric scan rate (ν) of 1 V s^{-1}.

microscopy (FE-SEM), as depicted in Fig. 1b and c. Considering Fig. 1b, the h-BN nanosheets are triangular in shape and show a much darker contrast compared to the underlying Cu support, with sizes ranging from *ca.* 5 to 12 μm, in agreement with previous reports.[23] It should be noted that the white particles on the h-BN/Cu surface are comprised of borazine, arising from the decomposition of the ammonium borane precursors.[24] Considering Fig. 1c, the morphology of transferred h-BN/Au is quite similar with that of h-BN/Cu, with h-BN nanosheets (dark regions in Fig. 1c) of approximately *ca.* 5 μm in size dispersed on the underlying Au support (light regions in Fig. 1c).

The electrocatalytic activity of h-BN/Cu towards the HER was screened using voltammetric SECCM, where hundreds of local (spatial resolution or 'hopping distance' of 500 nm) LSV measurements were performed with a nanopipet probe of $d_t \approx 300$ nm (see Fig. S1a of the ESI†). Note that the ORR was found to make a negligible contribution to the electrocatalytic current measured on the basal surface of h-BN/Cu during cathodic polarization, revealed by performing point measurements in an environmental chamber under an inert (argon) atmosphere (*i.e.*, in the presence and absence of air),[25,26] as explored in the ESI,† Section S2. For this reason, all SECCM experiments were carried out without environmental control (*i.e.*, in the presence of air), and the electrocatalytic current can be attributed to the HER alone. An FE-SEM image of the area scanned with SECCM is shown in Fig. 2a; the individual droplet 'footprints' are visible on the h-BN surface (light regions), as are exposed regions of the underlying Cu support (dark regions with sharp outlines). Representative LSVs, taken from 45 points across the h-BN surface and normalized by the area of individual footprints (Fig. 2a), as well as the average LSV recorded from all points on the surface of the h-BN nanosheets (684 individual measurements) are shown in Fig. 2b. The LSVs measured at h-BN/Cu are highly reproducible, reflected in the histogram constructed from the current density (j) measured at −0.688 V *vs.* the reversible hydrogen electrode (RHE), shown in Fig. 2c, which is Gaussian in shape (N = 684), with a peak (mean) value of 10 (±2) mA cm^{-2}.

The overpotential (η) required to achieve a j of 20 mA cm^{-2} (termed η_{20}) at h-BN/Cu is *ca.* −0.77 V, indicating that the HER is kinetically sluggish on this material. Although this value is much larger than literature values for HER nanocatalysts such as metallic WS_2 nanosheets on graphite[27] and nanocrystalline MoS_2 on Au,[4] such measurements were performed exclusively by bulk (macroscopic) measurements on ensembles of material, where the number (*i.e.*, surface area) and type (*i.e.*, basal plane *vs.* edge plane) of exposed surface site is not known, making normalization to the true electrochemical surface area (ECSA) impossible.

This is an important advantage of SECCM over macroscopic (bulk) voltammetry, as particular surface sites can be targeted (*i.e.*, the basal surface of h-BN), with the exposed surface area accurately known from the droplet 'footprint' (Fig. 2a), allowing the true intrinsic catalytic activity to be extracted by semi-quantitative Tafel analysis (*vide infra*).[19] In any case, it is worth noting that the η_{20} value measured at h-BN/Cu (−0.77 V) is much lower than the reported value of a BN-modified graphite electrode (−1.15 V),[28] indicating the underlying Cu substrate can promote the HER performance of h-BN, which is usually considered to be an insulator.

The electrocatalytic activity of h-BN/Au towards the HER was also screened using voltammetric SECCM ($d_t \approx 150$ nm, see Fig. S1b of the ESI†); an FE-SEM image of the scan area is shown in Fig. 2d. The dark regions represent the surface of the individual h-BN nanosheets, while the light regions correspond to exposed Au substrate (droplet 'footprints' also seen in the image). Representative LSVs, taken from 35 points across the surface of the h-BN nanosheets, as well as the average LSV recorded from all points on the surface of h-BN/Au (515 individual measurements) are shown in Fig. 2e. Evidently, the electrocatalytic activity of h-BN/Au for the HER is much higher than that of h-BN/Cu (albeit, still lower than the underlying Au support, see Section S3 in the ESI†), with an η_{20} value of −0.47 V for the former, compared to −0.77 V for the latter (*vide supra*). This is also reflected in the histogram constructed from the j values measured on h-BN/Au at −0.688 V *vs.* RHE, shown in Fig. 2f, which is also Gaussian in shape ($N = 515$), with a peak (mean) value of 900 (±200) mA cm^{-2}, approximately two orders of magnitude larger than that measured at h-BN/Cu. These results unequivocally demonstrate that interaction with the underlying metal support can have a significant effect on the electronic properties of h-BN, evident from the vastly different HER catalytic activities measured when supported on Au and Cu.

A direct comparison of the average area normalized LSVs measured on h-BN/Cu, h-BN/Au and the Au support substrate is shown in Fig. 3a. Evidently, while the measured j at a given potential is *ca.* 2 orders of magnitude larger on h-BN/Au compared to h-BN/Cu (*e.g.*, $j = 10$ and 900 mA cm^{-2} at −0.688 V *vs.* RHE on h-BN/Cu and h-BN/Au, respectively), the former material is still less active than the underlying Au substrate (*i.e.*, $j \approx 1600$ mA cm^{-2} at 0.688 V *vs.* RHE on Au). This was confirmed by semi-quantitative Tafel analysis, as shown in Fig. 3b. All materials possess similar Tafel slopes of *ca.* 120 mV per decade (136, 108 and 130 mV per decade at h-BN/Cu, h-BN/Au and Au, respectively), which is consistent with the rate determining step being the initial discharge of H^+ at the electrode surface (termed the Volmer step in the classical Volmer–Tafel–Heyrovsky mechanism of hydrogen evolution), although this conclusion should be treated *cum grano salis*, as the specific mechanism of the HER cannot be unambiguously determined from the Tafel slope alone.[19]

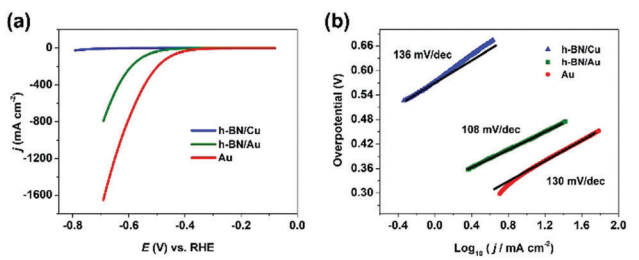

Fig. 3 (a) LSVs (area normalized) and (b) corresponding Tafel plots obtained from the HER on h-BN/Cu (blue curve), h-BN/Au (green curve) and Au substrate (red curve). These data were obtained from a 0.1 M $HClO_4$ solution at $\nu = 1$ V s^{-1}. Linear least-squares fit (black traces, slope indicated on plot) is also shown in (b).

The exchange current density (j_0), estimated directly by extrapolation of the linear Tafel region, reflects the relative catalytic activity of the materials, with values of *ca.* 4×10^{-8} A cm^{-2}, 1×10^{-6} A cm^{-2}, and 4×10^{-6} A cm^{-2} measured at h-BN/Cu, h-BN/Au and Au, respectively. As noted above, making a meaningful comparison between these data and literature data on h-BN is difficult, as the quantity and type of exposed surface site is often not known in macroscopic ensemble-type studies. Nevertheless, the Tafel slope and j_0 values measured in this study are far less favorable (in the catalytic sense) compared to those previously measured at macroscopic h-BN/Au ensembles, where optimal values of *ca.* 30 mV per decade and 4.6×10^{-5} A cm^{-2}, respectively were reported.[11] This suggests that the edges of h-BN, which would be exposed in the bulk measurements (as in ref. 11) but not the local ones (as carried out here), are likely to be predominantly responsible for the observed macroscopic activity in h-BN/Au ensembles. In any case, the j_0 of h-BN/Au is orders of magnitude lower than polycrystalline Pt ($j_0 = 3 \times 10^{-3}$ A cm^{-2}),[29] but is comparable to that measured on the basal plane of bulk (natural crystal) MoS_2 ($j_0 = 2.5 \times 10^{-6}$ A cm^{-2})[19] and a monolayer MoS_2 film supported on glassy carbon ($j_0 = 1.1 \times 10^{-6}$ A cm^{-2}).[30]

As a wide band gap semiconductor, h-BN in its native form is assumed to be electrochemically (and electrocatalytically) inert.[31] In this study, h-BN supported on either Cu or Au substrates exhibits moderate catalytic activity towards the HER, with the enhancement effect of Au being much more pronounced than that of Cu. From this, we conclude that the substrate-dependent HER activity of h-BN is attributable to the interaction with the underlying metal support, which tunes molecular processes such as surface diffusion, adsorption and on-surface (interfacial) reactions.[32] As alluded to above, it has been reported that the strength of chemical bonding at the interface of h-BN and transition metal substrates is determined mainly by the strength of the d and π orbital hybridization.[33,34] On Cu(111), h-BN has previously been shown to be only weakly chemisorbed,[35] evidenced by scanning tunneling microscopy and spectroscopy experiments.[36] On the other hand, theoretical calculations have predicted a perturbation of the electronic states of h-BN when interacting with an Au substrate.[9] This is consistent with the fact that various forms of BN (nanotubes, nanosheets and sputter deposited BN) have been shown to significantly lower the overpotential associated with ORR at Au substrates, but have either no or a hindering effect at glassy carbon and Pt electrodes, respectively.[37] It is generally accepted that the ideal HER electrocatalyst should possess a near thermoneutral free energy of adsorbed atomic hydrogen, that is, $\Delta G_H^* \approx 0$ eV.[38] We postulate that the significantly different HER activities of h-BN/Cu and h-BN/Au likely arise from different

ΔG_H^* values at these two substrates. In other words, electronic coupling of h-BN and Au might result in more optimal adsorption–desorption processes (*i.e.*, $\Delta G_H^* \rightarrow 0$), greatly facilitating the HER. On this basis, we propose that further theoretical studies of metal-support effects on ΔG_H^* at h-BN could be very interesting and usefully aid understanding in HER electrocatalysis at this type of nanomaterial.

In summary, SECCM has been employed to screen the intrinsic electrochemical activity (*i.e.*, HER electrocatalysis) of h-BN supported on Cu and Au substrates. Local voltammetric measurements revealed that the HER charge-transfer kinetics are *ca.* two orders of magnitude larger at the basal surface of h-BN when it is supported at Au (*i.e.*, h-BN/Au) compared to Cu (*i.e.*, h-BN/Cu). This significant enhancement was attributed to differences in the substrate effect between h-BN and Au/Cu, opening up the possibility of tuning reactivity (*e.g.*, catalytic activity) through the underlying metal support. Overall, these findings pave the way towards rational design of h-BN based electromaterials, with the ultimate goal being the replacement of noble metals with inexpensive and (electro)chemically stable metal-free counterparts in HER electrocatalysis.

PRU thanks the Royal Society for a Wolfson Research Merit Award and Industry Award (INF/R1/180026). DQL thanks the China Scholarship Council-Warwick joint scholarship programme. BT acknowledges support from a University of Warwick Chancellor's International Scholarship. CLB acknowledges financial support the European Union's Horizon 2020 research and innovation programme under the Marie Skłodowska-Curie grant agreement no. 702048 (NEIL) and the Ramsay Memorial Fellowship Trust.

Conflicts of interest

There are no conflicts to declare.

Notes and references

1 Y. Jiao, Y. Zheng, M. Jaroniec and S. Z. Qiao, *Chem. Soc. Rev.*, 2015, **44**, 2060–2086.
2 H. A. Gasteiger and N. M. Marković, *Science*, 2009, **324**, 48–49.
3 Q. Li, L. Wu, G. Wu, D. Su, H. Lv, S. Zhang, W. Zhu, A. Casimir, H. Zhu and A. Mendoza-Garcia, *Nano Lett.*, 2015, **15**, 2468–2473.
4 T. F. Jaramillo, K. P. Jørgensen, J. Bonde, J. H. Nielsen, S. Horch and I. Chorkendorff, *Science*, 2007, **317**, 100–102.
5 Y. Zheng, Y. Jiao, Y. Zhu, L. H. Li, Y. Han, Y. Chen, A. Du, M. Jaroniec and S. Z. Qiao, *Nat. Commun.*, 2014, **5**, 3783.
6 J. Yang, D. Voiry, S. J. Ahn, D. Kang, A. Y. Kim, M. Chhowalla and H. S. Shin, *Angew. Chem.*, 2013, **125**, 13996–13999.
7 D. Deng, K. Novoselov, Q. Fu, N. Zheng, Z. Tian and X. Bao, *Nat. Nanotechnol.*, 2016, **11**, 218–230.
8 V. Solozhenko, A. Lazarenko, J.-P. Petitet and A. Kanaev, *J. Phys. Chem. Solids*, 2001, **62**, 1331–1334.
9 K. Uosaki, G. Elumalai, H. Noguchi, T. Masuda, A. Lyalin, A. Nakayama and T. Taketsugu, *J. Am. Chem. Soc.*, 2014, **136**, 6542–6545.
10 R. Koitz, J. K. Nørskov and F. Studt, *Phys. Chem. Chem. Phys.*, 2015, **17**, 12722–12727.
11 K. Uosaki, G. Elumalai, H. C. Dinh, A. Lyalin, T. Taketsugu and H. Noguchi, *Sci. Rep.*, 2016, **6**, 32217.
12 S. Azevedo, J. Kaschny, C. De Castilho and F. de Brito Mota, *Eur. Phys. J. B*, 2009, **67**, 507–512.
13 J. Zhou, Q. Wang, Q. Sun and P. Jena, *Phys. Rev. B: Condens. Matter Mater. Phys.*, 2010, **81**, 085442.
14 L. Britnell, R. V. Gorbachev, R. Jalil, B. D. Belle, F. Schedin, M. I. Katsnelson, L. Eaves, S. V. Morozov, A. S. Mayorov and N. M. Peres, *Nano Lett.*, 2012, **12**, 1707–1710.
15 M. Gao, A. Lyalin and T. Taketsugu, *Int. J. Quantum Chem.*, 2013, **113**, 443–452.
16 N. Ebejer, A. G. Güell, S. C. S. Lai, K. McKelvey, M. E. Snowden and P. R. Unwin, *Annu. Rev. Anal. Chem.*, 2013, **6**, 329–351.
17 C. L. Bentley, M. Kang and P. R. Unwin, *Curr. Opin. Electrochem.*, 2017, **6**, 23–30.
18 C. L. Bentley, M. Kang and P. R. Unwin, *J. Am. Chem. Soc.*, 2017, **139**, 16813–16821.
19 C. L. Bentley, M. Kang, F. M. Maddar, F. Li, M. Walker, J. Zhang and P. R. Unwin, *Chem. Sci.*, 2017, **8**, 6583–6593.
20 C.-H. Chen, L. Jacobse, K. McKelvey, S. C. S. Lai, M. T. Koper and P. R. Unwin, *Anal. Chem.*, 2015, **87**, 5782–5789.
21 Y. Stehle, H. M. Meyer III, R. R. Unocic, M. Kidder, G. Polizos, P. G. Datskos, R. Jackson, S. N. Smirnov and I. V. Vlassiouk, *Chem. Mater.*, 2015, **27**, 8041–8047.
22 X. Li, Y. Zhu, W. Cai, M. Borysiak, B. Han, D. Chen, R. D. Piner, L. Colombo and R. S. Ruoff, *Nano Lett.*, 2009, **9**, 4359–4363.
23 N. Guo, J. Wei, L. Fan, Y. Jia, D. Liang, H. Zhu, K. Wang and D. Wu, *Nanotechnology*, 2012, **23**, 415605.
24 R.-J. Chang, X. Wang, S. Wang, Y. Sheng, B. Porter, H. Bhaskaran and J. H. Warner, *Chem. Mater.*, 2017, **29**, 6252–6260.
25 C.-H. Chen, K. E. Meadows, A. Cuharuc, S. C. S. Lai and P. R. Unwin, *Phys. Chem. Chem. Phys.*, 2014, **16**, 18545–18552.
26 B. D. B. Aaronson, S. C. S. Lai and P. R. Unwin, *Langmuir*, 2014, **30**, 1915–1919.
27 M. A. Lukowski, A. S. Daniel, C. R. English, F. Meng, A. Forticaux, R. J. Hamers and S. Jin, *Energy Environ. Sci.*, 2014, **7**, 2608–2613.
28 S. Wirth, F. Harnisch, M. Weinmann and U. Schröder, *Appl. Catal., B*, 2012, **126**, 225–230.
29 J. Greeley, T. F. Jaramillo, J. Bonde, I. Chorkendorff and J. K. Nørskov, *Nat. Mater.*, 2006, **5**, 909–913.
30 Y. Yu, S.-Y. Huang, Y. Li, S. N. Steinmann, W. Yang and L. Cao, *Nano Lett.*, 2014, **14**, 553–558.
31 G.-H. Yang, J.-J. Shi, S. Wang, W.-W. Xiong, L.-P. Jiang, C. Burda and J.-J. Zhu, *Chem. Commun.*, 2013, **49**, 10757–10759.
32 W. Auwärter, *Surf. Sci. Rep.*, 2018, DOI: 10.1016/j.surfrep.2018.10.001.
33 E. Rokuta, Y. Hasegawa, K. Suzuki, Y. Gamou and C. Oshima, *Phys. Rev. Lett.*, 1997, **79**, 4609–4612.
34 A. B. Preobrajenski, A. S. Vinogradov and N. Mårtensson, *Phys. Rev. B: Condens. Matter Mater. Phys.*, 2004, **70**, 165404.
35 A. Preobrajenski, A. Vinogradov and N. Mårtensson, *Surf. Sci.*, 2005, **582**, 21–30.
36 S. Joshi, D. Ecija, R. Koitz, M. Iannuzzi, A. P. Seitsonen, J. R. Hutter, H. Sachdev, S. Vijayaraghavan, F. Bischoff and K. Seufert, *Nano Lett.*, 2012, **12**, 5821–5828.
37 G. Elumalai, H. Noguchi and K. Uosaki, *Phys. Chem. Chem. Phys.*, 2014, **16**, 13755–13761.
38 J. D. Benck, T. R. Hellstern, J. Kibsgaard, P. Chakthranont and T. F. Jaramillo, *ACS Catal.*, 2014, **4**, 3957–3971.